Journal of
Synchrotron
Radiation

ISSN 0909-0495

Received 2 February 2007
Accepted 23 May 2007

Two-step hard X-ray focusing combining Fresnel zone plate and single-bounce ellipsoidal capillary

A. Snigirev,[a]* A. Bjeoumikhov,[b] A. Erko,[c] I. Snigireva,[a] M. Grigoriev,[d] V. Yunkin,[d] M. Erko[b] and S. Bjeoumikhova[e]

[a]ESRF, 6 rue Jules Horowitz, 38043 Grenoble, France, [b]IFG Institute for Scientific Instruments GbmH, Rudower Chaussee 29/31, 12489 Berlin, Germany, [c]BESSY GmbH, Albert-Einstein Strasse 15, 12489 Berlin, Germany, [d]IMT RAS, 132432 Chernogolovka, Moscow Region, Russia, and [e]Bundesanstalt fur Materialforschung and Prufung, 12200 Berlin, Germany. E-mail: snigirev@esrf.fr

A two-step focusing set-up combining a Fresnel zone plate with an ellipsoidal capillary is presented. It is shown that, in addition to the anticipated gain in flux, the employment of the prefocusing micro-optic makes optimal use of the elliptical shape of the capillary by almost eliminating aberrations. A small cross section of the prefocused beam allows a tiny fraction of the capillary surface to be selected, thus reducing the influence of slope errors. An X-ray beam with a 15 keV energy was focused down to a spot size as small as 250 nm, demonstrating the best value that has been achieved up to now for single-bounce capillaries. The use of an ellipsoidal capillary as a micromirror under off-axis illumination by microfocusing optics may open up new opportunities in nanofocusing developments.

© 2007 International Union of Crystallography
Printed in Singapore – all rights reserved

Keywords: hard X-ray focusing; single-bounce capillaries; Fresnel zone plate.

1. Introduction

Nowadays all three X-ray classical optical schemes (reflective, refractive and diffractive optics) can offer a focus spot size below 100 nm. Examples include Kirkpatrick–Baez (KB) mirrors (Mimura *et al.*, 2005), nanofocusing refractive lenses (Schroer *et al.*, 2005) and Fresnel zone plates (FZPs) (Kang *et al.*, 2006). Being a part of reflective optics, capillaries were already shown to have nanofocusing capabilities more than ten years ago (Bilderback *et al.*, 1994). Although the idea of using tapered glass capillaries looked very attractive, no appreciable progress in using such simple devices for nano-beams has been made so far since that time. The problems are well understood and consist of significant losses in the multi-reflection process and almost zero working distance, which substantially limits practical applications of capillaries in X-ray microscopy. However, single-bounce capillaries proposed by Balaic *et al.* (1995) show a great potential in developing nanofocusing techniques. Parabolic and elliptical capillaries have a large focal distance and very high reflectivity (Balaic *et al.*, 1995; Huang & Bilderback, 2003, 2006; Bartoll *et al.*, 2004; Bjeoumikhov *et al.*, 2005; Pinakidou *et al.*, 2006). In a typical process the predetermined capillary profile is achieved by 'pulling' an originally straight uniform glass tube with accurate control of mechanical movements and heating parameters. Unfortunately, owing to some unavoidable factors, *i.e.* surface slope errors of the original glass tube, temperature and density variations, and non-uniform mechanical movement, it is difficult to reliably achieve the elliptical shapes with the desired low-figure errors. State-of-the-art technology allows a capillary to be produced with 70 μm slope errors (Huang & Bilderback, 2006). To have a reasonable acceptance a typical capillary length ranges up to about 100 mm. Obviously such a distance of X-ray travelling through the capillary multiplied by the slope error limits the resolution of the optic by a size of about 10 μm.

To overcome these problems we propose to use a small elliptical capillary made using a stationary pulling technique, where the elliptical shape is achieved by stretching an air bubble inside a glass fiber with constant velocity (Knochel *et al.*, 1994). We believe that this approach shows a better quality surface compared with the computer-controlled glass-tube-pulling process at variable speed.

For best performance of the ellipsoidal capillary, we use a FZP lens to generate a secondary source at the first ellipse focus. It should be noted that secondary focusing using large capillaries has already been proposed but this had a modest resolution of about 20 μm (Huang & Bilderback, 2003). The possibilities of generating submicrometer beams using multi-bounce capillaries in conjunction with KB mirrors were discussed by Vincze & Riekel (2003). In our case the FZP serves as a first microfocusing element, producing a demagnified micrometer image of the source, and then the elliptical capillary makes a last final compression of the beam down to 250–500 nm. Such a stepwise focusing set-up offers, firstly, non-aberrational focusing by the elliptical capillary; secondly,

optimizing the overall acceptance of the optical system; and, thirdly, selecting the proper fraction of the capillary reflecting surface, minimizing figure errors.

2. Experiment and results

Experimental testing of the ellipsoidal capillary was performed at the Micro-optics test bench (MOTB) located 55 m from the source in the second experimental hutch of beamline BM5 at the ESRF (http://www.esrf.fr/UsersAndScience/Experiments/Imaging/BM05/BeamlineGuide/EH2/MicroOpticsTest/). The experimental set-up is shown in Fig. 1. White radiation from the bending magnet was collimated by primary and secondary slits and an incident X-ray energy of 15 keV was selected by using a water-cooled double-crystal Si(111) monochromator.

A silicon-based circular FZP (Snigireva *et al.*, 2007) was used to generate a secondary source at the first ellipse focus of the capillary. The FZP was manufactured using microelectronics and MEMS microfabrication technologies, including electron-beam lithography, photolithography and deep plasma etching of silicon. The main FZP parameters were: aperture A = 194 μm, outermost zone width Δr_n = 0.4 μm. The focal distance at 15 keV was 950 mm. The height of the FZP structure was 16 μm providing almost optimal diffraction efficiency at 15 keV. The FZP was mounted on the optics stage with necessary *X*-*Y*-*Z* translations. The motorized JJ slits were placed close to the FZP focus to select the first-order focusing and decrease the background from other orders.

A single-bounce hollow glass capillary was manufactured by 'pulling' a glass fiber with an air bubble inside (Knochel *et al.*, 1994). Drawing the fiber at a constant velocity in a hot area produced by an electrical heater obviously transfers the spherical shape of the bubble into an elliptical shape. As a result an ellipsoidal capillary was created with the following ellipse dimensions: major axis $2a$ = 95 mm and minor axis $2b$ = 50 μm. It is clear that such a high-aspect-ratio ellipse has foci very close to the tips of the ellipse, and the distance between foci is practically equal to the size of the major axis, $2a$ = 95 μm.

This ellipsoidal capillary was first divided in half with an entrance diameter of 50 μm, and then one half was cut so as to have an output diameter of 8 μm providing a working distance of 0.6 mm. Finally the remaining elliptical capillary with a length of 46.9 mm was used. The capillary was mounted in a V-groove located on the optics stage with six degrees of freedom (three translations and three rotations).

A high-resolution X-ray Sensicam CCD camera with 1.3 μm resolution (0.65 μm pixel size) was positioned beyond the capillary to observe the far-field pattern of radiation emerging from the capillary. The camera was used to align the optic, as well as to determine its quality from the uniformity and symmetry of the pattern. The lateral size of the microbeam was measured by scanning a 200 μm-diameter Au wire across the beam vertically, recording the transmission intensity using a standard Si pin-diode. The knife-edge was placed on a *Y*-*Z* piezo-driven translation stage having a repeat accuracy of better then 30 nm. The piezo stage was mounted on top of the MOTB scanning stage with three translational and one rotational degrees of freedom. The knife-edge was aligned with the X-ray CCD camera.

Prior to testing the capillary we measured the effective source size using the interferometric technique described by Kohn *et al.* (2000). The measured source size was 120 μm vertically and 250 μm horizontally. The vertical source size is larger than the original one. It is known that monochromator vibrations are responsible for the increase in the source size. Since the vertical beam size is smaller, we made all measurements of the capillary focusing in the vertical direction only.

First we aligned and tested the focusing properties of the ellipsoidal capillary using a flat parallel 15 keV beam from the monochromator (Fig. 2*a*). In this case JJ slits were placed close to the capillary entrance to limit the incident X-ray beam so that it slightly overfills the optic entrance aperture. It should be mentioned that the capillary annular ring of approximately 2 μm around the exit does not reflect the 15 keV beam owing to the critical angle. The focal spot measured by knife scan shows a 2 μm FWHM (full width at half-maximum) size in the vertical direction. Obviously focusing is limited by the aberrations of the elliptical shape of the optic for the incident parallel illumination. In addition, the intensity profile of the focused beam showed the 8 μm pedestal created by the direct X-rays passing through the capillary tip opening. The result perfectly matched the ray-tracing calculations made using the code *RAY* developed at BESSY for beamline design calculations (Schaefers, 1996).

Switching to the optimal situation, the circular FZP was used to generate a secondary source exactly at the position of the first focus of the capillary at a distance of 47.5 mm from the entrance. The secondary source produced by the FZP and evaluated using the knife-edge technique was 2.2 μm vertically and 5 μm horizontally (FWHM). Taking into account the demagnification factor $M_1 = L_1/L_2$ = 55/0.95 = 58, these values are in a very good agreement with the expected ones. The measured FZP efficiency was about 27%.

Having the FZP on an axis with the capillary (Fig. 2*b*), the footprints of the beam in the vertical direction at the capillary entrance and the exit are

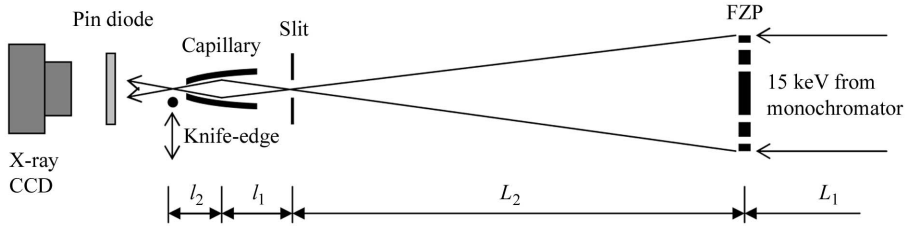

Figure 1
Two-step focusing experimental set-up. L_1 = 55 m is the source distance, *i.e.* the distance from the bending magnet source to the FZP position, L_2 = 0.95 m is the image distance. l_1 is the secondary source distance and l_2 is the secondary image distance.

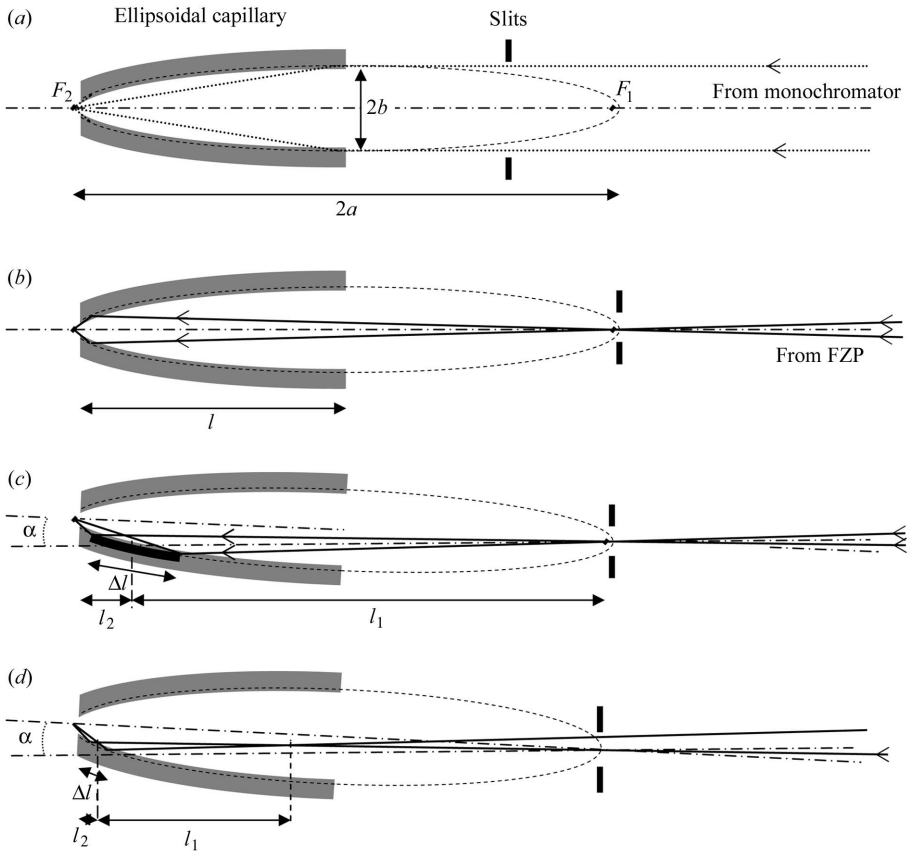

Figure 2
Schematic of the capillary focusing with (*a*) parallel (direct) illumination, (*b*) FZP pre-focus beam in the first capillary focus with in-axis illumination, (*c*) FZP pre-focus beam at the position of the first focus of the capillary at a distance of 47.5 mm from the entrance with off-axis illumination, (*d*) FZP pre-focus beam inside the capillary with off-axis illumination. F_1 and F_2 are foci of the ellipsoidal capillary, *a* and *b* are the lengths of the semi-major and semi-minor ellipse axes, respectively, *l* is the capillary length, Δl is the footprint of the beam impinging on the surface of one side of the capillary (heavy weight curve), l_1 is the distance from the FZP focus to the mid-position of the beam footprint on the capillary surface, l_2 is the distance from the mid-position of the footprint of the beam to the capillary focus, and α is the capillary tilt angle around the first focal point F_1.

10 μm and 20 μm, respectively. With such an arrangement we do not illuminate the whole capillary inner surface but only a small section of the capillary close to its exit, with a length of about 5 mm. For simplicity, let us count the image distance from the mid-position of this ring. Under these conditions the demagnification factor for the capillary is $M_2 = l_1/l_2 = 92.5/2.5 = 37$. Combined with the FZP, the demagnification power of the entire system will then be $M = M_1M_2 = 2150$. The geometrically demagnified beam should have a FWHM of less than 100 nm. Instead, the experimentally measured focal spot was about 1 μm. Such discrepancy can be explained by average slope errors of the capillary consisting of figure and centerline straightness (or circular symmetry) errors (Huang & Bilderback, 2006). It is known that the present technology allows capillaries to be produced with average slope errors in the 70 μrad range (25–50 μrad for figure errors and 68 μrad for straightness errors). One should not exclude the fact that scattering at the edge of the capillary bore can result in a broadening of the focal spot. Besides, a direct beam from the FZP passing through the capillary opening without being reflected increases the background.

Taking advantage of the tiny focus beam generated by the FZP, we use an off-axis focusing geometry. For this we have tilted the capillary around the first focus point so that only a small part of the capillary side wall is involved in the reflection (see Fig. 2*c*). In fact, by changing the tilt angle, we can vary the position of the beam on the capillary surface and therefore we can easily control the demagnification factor M_2. Owing to off-axis illumination, we used only one side of the capillary and in this way the influence of centerline straightness errors and scattering at the edge of the capillary bore are eliminated. With a tilt angle of 0.16 mrad and a beam footprint of about 15 μm the 18 mm-long mirror-like surface of the capillary was illuminated. Under these circumstances the image distance counted from the mid-position of such an extended mirror corresponds roughly to 9 mm and the demagnification factor can be estimated as $M_2 = 86/9 = 9.6$. Taking into account a secondary source size of 2.2 μm, a focal spot of the order of 0.23 μm might be expected. We measured the focal spot to be about 0.5 μm (FWHM). Increase in the beam footprint up to 20 μm for a tilt angle of 0.2 mrad leads to a focal spot of 0.8 μm, while a geometrically demagnified spot was expected of the order of 0.4 μm. The fact that the measured focal spot in both cases is slightly larger than expected is attributable to the slope errors of the capillary surface. In such an arrangement the focus blurring is mainly due to the capillary figure errors and becomes more pronounced when we illuminate a larger area on the capillary surface.

In order to illuminate a still smaller area of the capillary surface and to reduce the influence of the slope errors, we move the FZP focal spot inside the capillary at a distance of 30 mm from the capillary exit (Fig. 2*d*). It should be noted that in this case the footprint of the beam at the capillary exit in the vertical direction is about 6 μm, *i.e.* is smaller than the exit aperture of the capillary. By tilting the capillary at an angle of 0.08 mrad, we illuminate a 5 mm-long section of the capillary surface. At this position, the capillary will demagnify the intermediate spot further by a factor $M_2 = 27.5/2.5 = 11$. Fig. 3 depicts the vertical knife scan together with the extracted beam profile observed. The FWHM of the beam is 250 nm. A focus spot of around 200 nm was expected for an ideal capillary. Discordance between the measured and expected beam can be attributed to capillary local figure errors. We assume that in this case the measured focal spot is a convolution of the

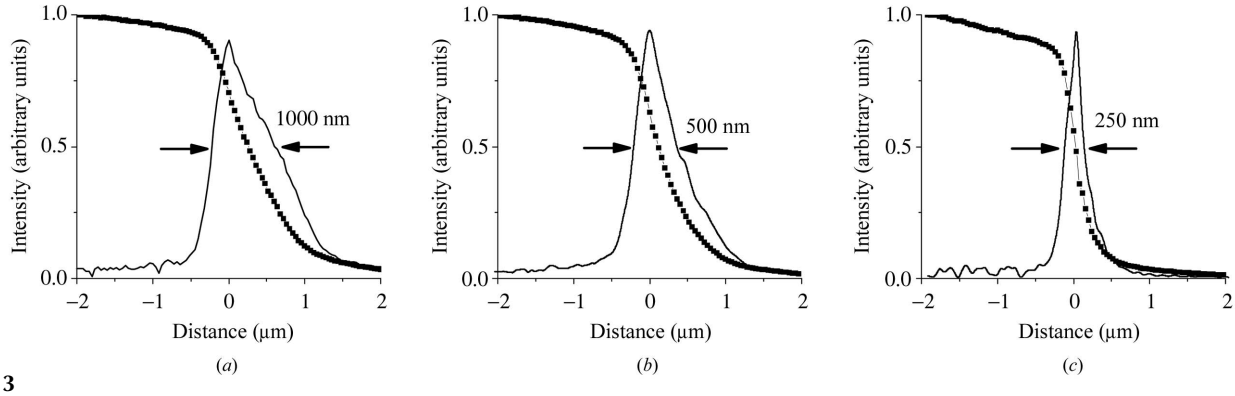

Figure 3
Vertical scans of a 200 μm Au wire as a knife-edge through the microbeam with extracted beam profiles measured according to the set-up in (*a*) Fig. 2(*b*), (*b*) Fig. 2(*c*) and (*c*) Fig. 2(*d*).

geometrically demagnified source size with local surface slope errors. Simple estimations show that 25 μrad figure errors add an additional focus blurring of about 125 nm. Adding in quadrature the slope-error blurring to the geometrical image of 200 nm we obtain an image size of 250 nm. This is in excellent agreement with the measured spot size. The size of the focus beam becomes larger as the tilt angle increases further. A beam size in the 380 nm range was observed for a tilt angle of 0.1 mrad, where the 8 mm-long capillary section works. The geometrically demagnified beam should have a FWHM of less then 340 nm in the vertical direction.

In the case where FZPs are used, a flux enhancement by almost a factor of four in comparison with single capillary focusing was measured. This is in good agreement with the predicted enhancement taking into account that the FZP efficiency is 27% and that the aperture is about four times larger then the capillary acceptance. The overall gain of the two-step focusing system was higher than 1000 compared with a flat monochromatic beam.

3. Discussion and conclusion

In general, the above-described two-step focusing set-up provides three important benefits: (i) it significantly improves the flux by increasing the overall acceptance of the optical system; (ii) it allows optimal aberration-free focusing by the elliptical capillary surface, and (iii) it considerably minimizes the influence of capillary figure errors. The proposed off-axis geometry allows the influence of the capillary centerline straightness slope errors on the focusing performance to be eliminated. This is the major problem associated with the glass capillary technology which limits the application of single-bounce capillaries for nanometer-focusing capabilities. It is obvious that the capillary straightness determines the focal spot and it has to be smaller or comparable with a desired focal spot. For nanofocused capillaries, the straightness and the capillary round symmetry has to be at the nanometer level that is evidently not realised with the present glass-pulling technology.

For practical applications, off-axis illumination of the capillary by a small prefocused beam brings some other advantages. It eliminates the beam transmitted through the exit aperture, aids the removal of harmful scattering by edges at the capillary tip and makes for an easy implementation of a beamstop. The off-axis micro-illumination arrangements may add some tunability to the microprobe. By accurate scanning of the tiny beam along the capillary surface one can control the demagnification factor and zoom the focal spot. By tilting the capillary, the incident angle can be changed and therefore energy cut-off can be controlled.

It is to be noted that the proposed approach allows an already small capillary to be shortened further down to 5–10 mm, making it easy to align and operate. Such small capillaries can even be bundled up in a tiny revolver-type assembly providing an easy switch to a proper capillary for a desired energy or working distance. The extreme compactness of the capillary might significantly simplify the mechanics in terms of alignment, permitting easy integration with a sample scanning system. Use of short capillaries might open the possibility of coating the inside of capillaries with metal films of desirable materials such as platinum or gold. The possibility of opening a capillary from one side by special cutting, etching or polishing may not be ruled out, which might also facilitate the coating process. In this way, metal capillary optics looks very attractive (Hirsch, 2003).

In addition, the availability of two focused spots in a two-step focusing set-up can offer an easy switch between submicrometer-probe and nanoprobe modes, moving a capillary in and out with a relatively small correction of optics or sample position. Optionally, the in-line full-field imaging and tomography using a conical or flat coherent beam is straightforward in this arrangement as well. The single-bounce ellipsoidal capillaries are very attractive for X-ray microscopy techniques because they are so simple and have the potential to be reproduced inexpensively.

It should be mentioned that for two-step focusing set-ups refractive lenses or KB mirror/multilayer systems can be used as the first optical element as well. Concerning compound refractive lenses, their efficiency and gain might be much higher compared with FZPs for hard X-rays. In addition, parabolic refractive lenses do not generate high diffraction orders. In the case of spectroscopy applications, KB mirrors as prefocusing optics are more preferable owing to the energy tunability.

Finally, the proposed two-step focusing approach can be readily applied for nanofocusing schemes which are now under intensive developments at different synchrotron radiation facilities. In order to cancel the contribution of the source size and to provide a diffraction-limited resolution, a high demagnification factor is required. As a result, practically all promising nanofocusing devices have a very short focal length and therefore a very small effective aperture, which is typically less then 100 μm. Using a prefocusing optic with an effective aperture approximately equal to the spatial or transverse coherence length of the incoming beam might considerably improve the overall gain of the nanoprobe without losing the nanometer resolution.

The authors wish to thank the BM05 staff for the support during the experiment. MG and VY also acknowledge support from the INTAS postgraduate studentship program (INTAS 05-109-4444) and from the Russian Foundation for Basic Research (grant RFBR 07-02-00741 and MK-7207.2006.2).

References

Balaic, D. X., Nugent, K. A., Barnea, Z., Garret, R. & Wilkins, S. W. (1995). *J. Synchrotron Rad.* **2**, 296–299,

Bartoll, J., Röhrs, S., Erko, A., Firsov, A., Bjeoumikhov, A. & Langhoff, N. (2004). *Spectrochim. Acta B*, **59**, 1587–1592.

Bilderback, D. H., Hoffman, S. A. & Thiel, D. J. (1994). *Science*, **263**, 201–203.

Bjeoumikhov, A., Bjeoumikhova, S. & Wedell, R. (2005). *Part. Part. Syst. Char.* **22**, 384–390.

Hirsch, G. (2003). *J. X-ray Spectrom.* **32**, 229–238.

Huang, R. & Bilderback, D. (2003). *AIP Conf. Proc.* **705**, 712–715.

Huang, R. & Bilderback, D. (2006). *J. Synchrotron Rad.* **13**, 74–84.

Kang, H. C., Maser, J., Stephenson, G. P., Liu, C., Conley, R., Macrander, A. T. & Vogt, S. (2006). *Phys. Rev. Lett.* **96**, 127401.

Knochel, A., Gaul, G. & Lechtenberg, F. (1994). German Patent DE4444102C2.

Kohn, V., Snigireva, I. & Snigirev, A. (2000). *Phys. Rev. Lett.* **85**, 2745–2748.

Mimura, H. S. *et al.* (2005). *Jpn. J. Appl. Phys.* **44**, L539–L542.

Pinakidou, F., Katsikini, M., Paloura, E. C., Kavouras, P., Komninou, Ph., Karakostas, Th. & Erko, A. (2006). *Nucl. Instrum. Methods*, B**246**, 238–243.

Schaefers, F. (1996). *RAY. BESSY Ray-Trace Program to Calculate Synchrotron Radiation Beamlines.* BESSY Technischer Bericht TB 202, 1–37. BESSY, Berlin, Germany.

Schroer, C. G., Kurapova, O., Patommel, J., Boye, P., Feldkamp, J., Lengeler, B., Burghammer, M., Riekel, C., Vincze, L., Van der Hart, A. & Kuchler, M. (2005). *Appl. Phys. Lett.* **87**, 124103.

Snigireva, I., Snigirev, A., Vaughan, G., Di Michiel, M., Kohn, V., Yunkin, V. & Grigoriev, M. (2007). *AIP Conf. Proc.* **879**, 998–1002.

Vincze, L. & Riekel, C. (2003). *X-ray Spectrom.* **32**, 208–214.